catalysts

MDPI

*Article*

# The Mitigation of CO Present in the Water–Gas Shift Reformate Gas over IR-$TiO_2$ and IR-$ZrO_2$ Catalysts

**Ziyaad Mohamed, Venkata D. B. C. Dasireddy, Sooboo Singh and Holger B. Friedrich ***

Catalysis Research Group, School of Chemistry and Physics, Westville Campus, University of KwaZulu-Natal, Durban 4000, South Africa; chemcatm@gmail.com (Z.M.); dasireddy@gmail.com (V.D.B.C.D.); Singhso@ukzn.ac.za (S.S.)

* Correspondence: friedric@ukzn.ac.za; Tel.: +27-31-260-3107; Fax: +27-31-260-3091

**Abstract:** CO hydrogenation and oxidation were conducted over Ir supported on $TiO_2$ and $ZrO_2$ catalysts using a feed mimicking the water–gas shift reformate stream. The influence of the support interaction with Ir and the catalysts' redox and CO chemisorption properties on activity and selectivity were evaluated. Both catalysts oxidised CO to $CO_2$ in the absence of $H_2$, and a conversion of 70% was obtained at 200 °C. For the CO oxidation in the presence of $H_2$ over these catalysts, the oxidation of $H_2$ was favoured over CO due to $H_2$ spillover occurring at the active metal and support interface, resulting in the formation of interstitials catalysed by Ir. However, both catalysts showed promising activity for CO hydrogenation. Ir-$ZrO_2$ was more active, giving 99.9% CO conversions from 350 to 370 °C, with high selectivity towards $CH_4$ using minimal $H_2$ from the feed. Furthermore, results for the Ir-$ZrO_2$ catalyst showed that the superior activity compared to the Ir-$TiO_2$ catalyst was mainly due to the reducibility of the support and its interaction with the active metal. Controlling the isoelectric point during the synthesis allowed for a stronger interaction between Ir and the $ZrO_2$ support, which resulted in higher catalytic activity due to better metal dispersions, and higher CO chemisorption capacities than obtained for the Ir-$TiO_2$ catalyst.

**Keywords:** iridium; preferential oxidation; hydrogenation; spillover; isoelectric point



**Citation:** Mohamed, Z.; Dasireddy, V.D.B.C.; Singh, S.; Friedrich, H.B. The Mitigation of CO Present in the Water–Gas Shift Reformate Gas over IR-$TiO_2$ and IR-$ZrO_2$ Catalysts. *Catalysts* **2021**, *11*, 1378. https://doi.org/10.3390/catal11111378

Academic Editors: Jean-François Lamonier, Antonella Gervasini and Sebastiano Campisi

Received: 30 September 2021
Accepted: 7 November 2021
Published: 15 November 2021



## 1. Introduction

In the transition to the hydrogen economy from current power sources, proton exchange membrane fuel cells (PEMFC) are considered good candidates for portable power generation [1,2]. During onboard reforming of hydrogen for these fuel cells, trace amounts of CO are still present in the reformate feed following the water–gas shift (WGS) reaction. Preferential oxidation (PROX) and methanation (MET) of CO are viable processes employed to reduce the CO concentration to acceptable levels, feeding onboard PEMFCs with pure hydrogen, and thus avoiding unwanted poisoning by CO of the Pt anode [3–8].

These reactions have been widely studied using Au, Pt, Ru, Rh, Pd, Ir, Ni, Cu, and Co supported on non-reducible oxides [5,9–16]. Among these catalytic formulations, supported Ir catalysts have not been widely explored for the PROX reaction [13,17,18]. Nguyen et al. [18] showed that Ir supported on $Al_2O_3$ was less active than its ceria-supported counterparts (Pt, Pd and Ir) for the PROX reaction. Furthermore, the stability of the ceria supported Ir, compared to Rh and Ru, was much higher above 200 °C, since Rh and Ru, although encouraging CO dissociation, followed the methanation pathway.

Huang et al. [17] reported that Ir-$CeO_2$ catalysts, prepared by the deposition–precipitation method with no $Cl^-$ residue, gave the highest activity for the preferential oxidation reaction compared to the other prepared materials on metal oxides ($Al_2O_3$ and $TiO_2$). Additionally, reductive pre-treatment of the catalyst was necessary for attaining high activity on a sample containing 1.60 wt.% Ir. The catalyst gave the highest oxidation activity of 60%, which decreased with the temperature above 120 °C.

Ir supported on $ZrO_2$ has not been reported for these oxidation reactions. To the best of our knowledge, no data has been reported for Ir supported on $TiO_2$ and $ZrO_2$ for the CO hydrogenation reaction. Additionally, the effect of controlling the isoelectric point of the two supports during the synthesis of these catalysts has not been mentioned. This motivated the present study in which $TiO_2$ and $ZrO_2$ supported Ir (1 wt.%) was tested for both the oxidation and hydrogenation of CO in a feed mimicking the water–gas shift reformate. In addition to this, we emphasise the strong metal–support interaction effects on both the supports during these reactions. For catalyst preparation, the deposition–precipitation method was used. Recently, Doustkhah et al. [19] showed that using a $Cl^-$ containing medium in the catalyst preparation could generate oxygen vacancies. The effects shown by controlling the isoelectric points during catalyst synthesis were investigated.

## 2. Results and Discussion

### *2.1. Catalyst Characterisation*

#### 2.1.1. Physisorption and Elemental Analysis of the Materials

Table 1 shows the ICP and physisorption analysis results of bare supports and Ir- $TiO_2$ and Ir-$ZrO_2$ catalysts. The Ir wt.% loadings were the same for both catalysts and close to the nominal loading of 1%. The surface areas and pore volumes of the catalysts show a decrease compared to the supports. The decrease in pore volume could be evidence of the metal being on the support surfaces, and in the pores, to a degree. This effect is larger in the $TiO_2$ supported catalyst. Figure 1 shows the $N_2$ adsorption/desorption isotherms for the supports and catalysts studied. These isotherms correspond to type IV with H1 hysteresis, indicative of cylindrical bottle pores characteristic of mesoporous materials [20–23]. No significant changes can be observed regarding the isotherm shape following the addition of Ir, which confirms that the metal is located mainly on the surface of the supports and does not disrupt the pore structures. The pore size distributions in Figure 2 show no evident peaks corresponding to micropores or macropores for these materials, indicating that all materials have uniform mesoporosity. Slight shifts in the pore volumes are indicative of the presence of the metal on the supports.

**Table 1.** BET and ICP data of the supported Ir catalysts.

| Catalyst | Surface Area ($m^2/g$) | Pore Volume ($cm^3/g$) | Ir wt. (%) [a] |
|---|---|---|---|
| $TiO_2$ | 151 | 0.35 | - |
| $ZrO_2$ | 57 | 0.25 | - |
| Ir-$TiO_2$ | 95 | 0.23 | 1.1 |
| Ir-$ZrO_2$ | 50 | 0.23 | 1.1 |

[a] ICP analysis.

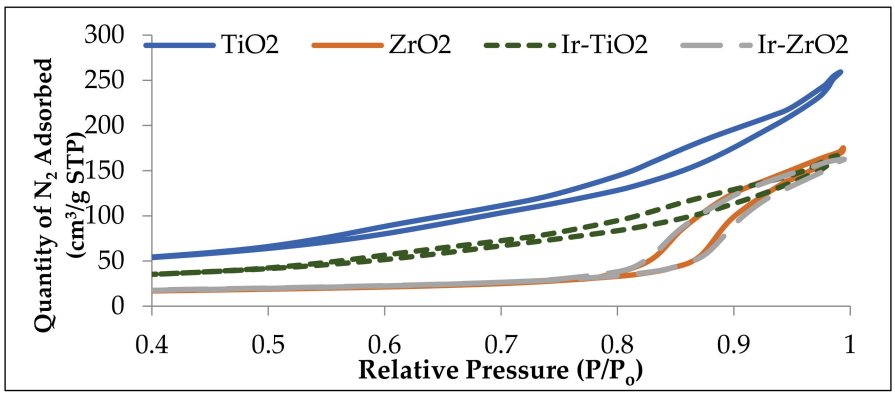


**Figure 1.** $N_2$ adsorption/desorption profiles of the materials.

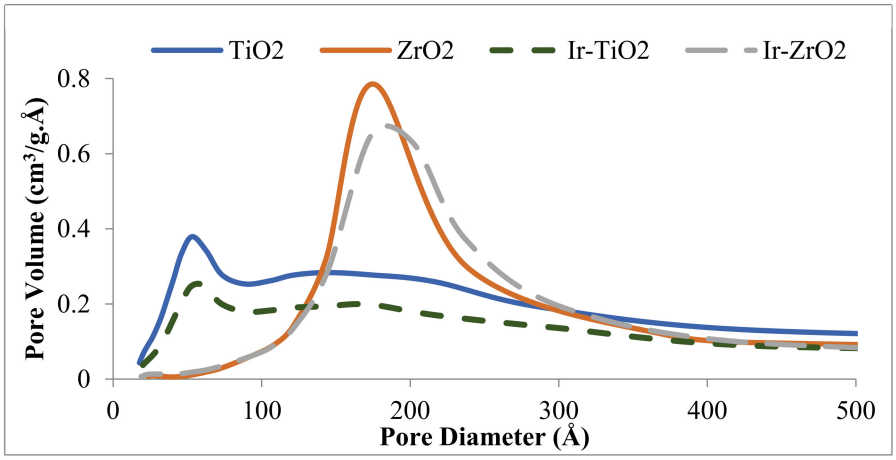


**Figure 2.** Pore size distributions of the materials.

2.1.2. Powder X-ray Diffraction

The X-ray diffractograms of the $TiO_2$ and $ZrO_2$ supported Ir catalysts (ESM, Figure S1) show no phases for Ir at these low weight loadings. This is generally the case for well-dispersed active phases, which XRD does not detected. It may be possible that Ir nanoparticles crystallised uniformly and occupied the pores of the support. Peaks characteristic of the supports, anatase (ICDD File No: 01-089-4921), and the monoclinic and tetragonal phases of $ZrO_2$ (ICDD File Nos: 01-074-1200 and 01-080-255), respectively, are seen.

2.1.3. X-ray Photon Spectroscopy

Peaks representative for the iridium oxide phases that XRD did not detect were confirmed using XPS. Figure 3 shows the deconvoluted Ir4$f_{7/2}$ XPS scan for the supported oxide catalysts. No peaks were observed at binding energies of ~60 eV corresponding to $Ir^0$. Peaks observed at binding energies of ~62 eV and ~64.7 eV are attributed to the $IrO_2$ phase. The binding energies also coincide with Ir 4$f_{7/2}$, which suggests that Ir is present in the $IrO_2$ phase [24,25]. Table 2 gives the binding energies observed for the Zr 3$d_{5/2}$, Ti 2$p_{3/2}$, Ir 4$f_{7/2}$, and O 1$s$, of the supported Ir catalysts. The binding energies of Zr 3$d_{5/2}$ at 184-188 eV, and Ti 2$p_{3/2}$ at 458-464 eV, are the expected values for the oxide supports [8,25,26] (ESM, Figure S2). The O 1$s$ spectra (ESM, Figure S2) of the supported Ir catalysts, and the binding energies obtained, correspond to two types of oxygen species, assigned to M-O-M (M = Ti or Zr) and Ir-O species on the support [21,25]. The Ir loadings obtained are also in agreement with the ICP values.

**Table 2.** XPS binding energies of the Ir-$TiO_2$ and Ir-$ZrO_2$ catalysts.

| Catalyst | Binding Energy (eV) | | | | Ir wt. % |
|---|---|---|---|---|---|
| | Ir (4$f_{7/2}$) | O (1$s$) | Ti (2$p_{3/2}$) | Zr (3$d_{5/2}$) | |
| Ir-$TiO_2$ | 62.3 | 529.3 | 458.8 | - | 0.9 |
| | 64.6 | | 464.1 | - | |
| Ir-$ZrO_2$ | 62.3 | 534.3 | - | 184.3 | 1.0 |
| | 64.8 | | - | 188.1 | |

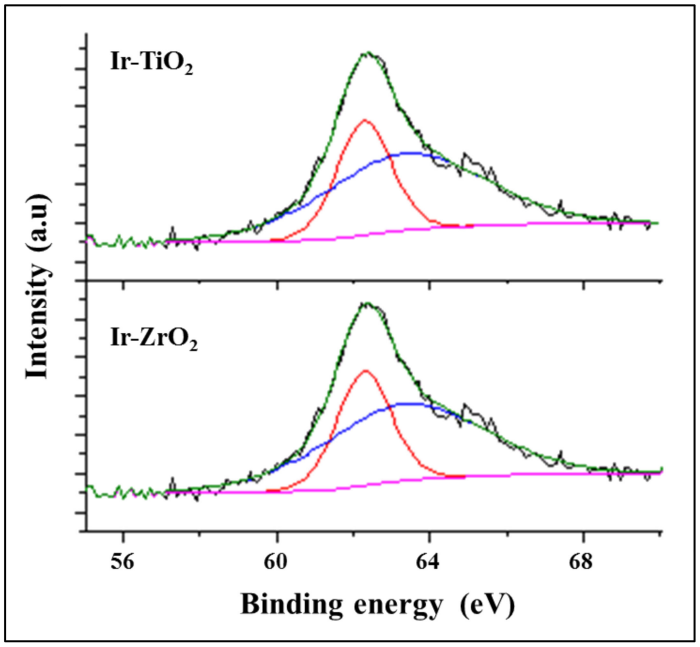


**Figure 3.** XPS spectra of the Ir4$f_{7/2}$ transition of Ir-$TiO_2$ and Ir-$ZrO_2$.

2.1.4. Temperature Programmed Studies

Temperature programmed reduction ($H_2$-TPR) profiles of the Ir-$TiO_2$ and Ir-$ZrO_2$ catalysts are shown in Figure 4. TPR of the bare supports did not show any peaks, which indicates that the peaks for the Ir-$TiO_2$ and Ir-$ZrO_2$ catalysts' $H_2$-TPR profiles are due to the presence of Ir in the catalyst. The catalysts have their main reduction peak at 113 °C (Ir-$TiO_2$) and 117 °C (Ir-$ZrO_2$), respectively. These peaks are attributed to the reduction of $IrO_2$ to metallic Ir. The reduction peak at 240 °C (Ir-$TiO_2$) could be due to the reduction of IrOx species with weak and medium interactions with the support [26]. The Ir-$ZrO_2$ catalyst has a shoulder peak at 167 °C with a broad reduction zone, which could reduce Ir oxide species with different interactions with $ZrO_2$ [27]. Reduction peaks observed for both of the catalysts above 300 °C could be attributed to the surface oxygen of the supports, or reduction by $H_2$ spillover [22,23,28–32]. Yoshida et al. [24] reported the formation of partially reduced $TiO_2$ by $H_2$ in Ir-$TiO_2$ catalysts, and a well-known phenomenon referred to as the strong metal–support interaction.

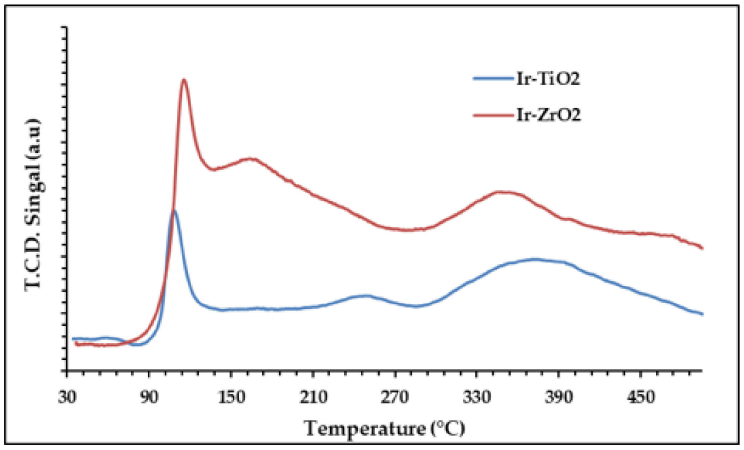


**Figure 4.** Temperature programmed reduction ($H_2$-TPR) profiles of the Ir-$TiO_2$ and Ir-$ZrO_2$ catalysts.

Similarly to the observed profiles in the literature [29,30,33–35], under reducing environments, reducible supported PGM metals with strong metal–support interactions tend

to become partially decorated by support interstitials that migrate towards and/or over the active metal at the metal–support interface. These migrations are not evident on bare supports but rather are catalysed by the active metal (Ir) as $MO_{(2-x)}$ species (M = Ti or Zr), as explained in various works [11,36]. This could be due to the initial reduction of metal species that strongly interact with the surface of the support. The use of acidic precursors ($Cl^-$) in the synthesis could also result in strong metal–support interactions between the metal and the surface of the support [37]. The TPR profiles of the Ir-$TiO_2$ and Ir-$ZrO_2$ materials show that Ir might be present in two locations, i.e., (i) on the surface of the support, and (ii), partially or completely entrenched within the support. Due to the presence of Ir at different locations on and within the support, Ir particles are reduced at different reduction temperatures.

Figure 5 shows the TPO profiles of the reduced catalyst samples. As with the Pt catalysts that we reported previously [11,36], the oxidation of these materials occurs readily at low temperatures even before the TCD records the signal. Also, according to the literature, highly dispersed Ir samples were found to be easily oxidised at low temperatures, from $Ir^0$ to $IrO_2$ [38]. $O_2$ consumption was still visible at higher temperatures, which could be evidence for the oxidation of the supports in close proximity to the metal that forms interstitial species.

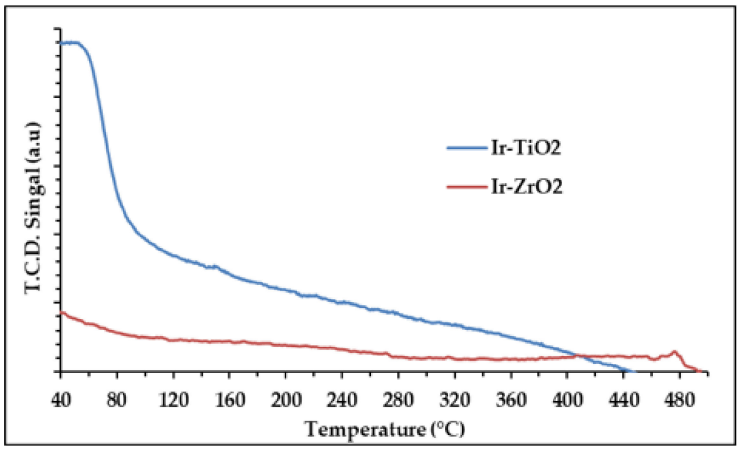


**Figure 5.** Temperature programmed oxidation ($O_2$-TPO) profiles of the Ir-$TiO_2$ and Ir-$ZrO_2$ catalysts.

### 2.1.5. FTIR-CO

An FTIR-CO analysis of the catalysts was used to determine the interaction of the metals with CO as the probe molecule. Figure S3 (ESM) shows the spectra obtained with increasing temperatures. Figure 6 shows the FTIR-CO analyses of the Ir-$TiO_2$ and Ir-$ZrO_2$ catalysts at a temperature of 200 °C. Both spectra show broad peaks for the supported catalysts at wavenumbers ~2050 $cm^{-1}$ (Ir-$ZrO_2$) and ~2060 $cm^{-1}$ (Ir-$TiO_2$), and a smaller shoulder band at ~1950 $cm^{-1}$. These bands indicate adsorption of CO over different metallic species of Ir present on the materials. It is reported that linear adsorption of CO to Ir sites ($Ir^0$–CO) can give a broad single band between 2000 and 2100 $cm^{-1}$ [27,39]. Furthermore, bands in the region of 2080 and 2010 $cm^{-1}$ (seen as shoulders on the main peak) could be assigned for concurrent adsorption of two CO molecules on Ir metallic sites [39]. The shoulder peak observed at ~1950 $cm^{-1}$ could be due to bridged CO molecules adsorbed on supported $Ir^0$ sites [40].

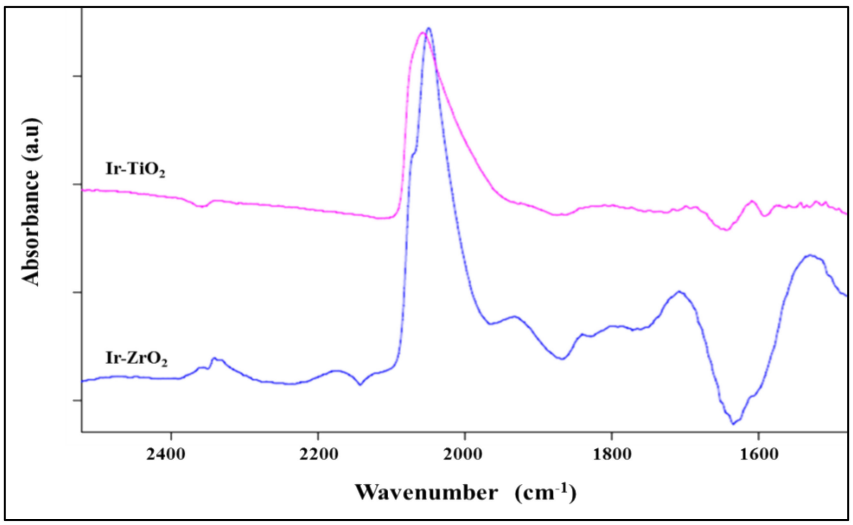


**Figure 6.** Fourier Transform Infrared-CO spectra of the Ir-$TiO_2$ and Ir-$ZrO_2$ catalysts (at 200 °C).

#### 2.1.6. CO Chemisorption

The CO chemisorption properties of the $TiO_2$ and $ZrO_2$ supported Ir catalysts at different reducing temperatures are depicted in Table 3. There was no CO chemisorbed on the bare supports during the CO chemisorption studies, thus, the results obtained over the catalysts are attributed to the Ir present on the respective supports. Similarly to the data presented for the Pt systems [11,36], the CO chemisorption capacity, metallic surface area, and metal dispersion, decrease with increasing reduction temperature. The Ir-$ZrO_2$ catalyst showed much better CO chemisorption capacity, metallic surface area, metal dispersion, and smaller crystallite sizes, than the $TiO_2$ supported catalyst. This result is also possibly due to the acidic Ir precursor ($IrCl_3$) used to synthesise these catalysts, which results in stronger interactions with the $ZrO_2$ support since it is more electropositive and basic than $TiO_2$ [41]. Additionally, the synthesis pH plays a significant role in controlling the zeta potential of these two supports, whereby the $ZrO_2$ at its isoelectric point (IEP) (pH 7.4) has a higher probability of metal interaction with the surface of the $ZrO_2$ (pH 5.5) than the $TiO_2$ (pH 6.0) [42]. As a result, the metallic surface areas, metal dispersions, and the CO chemisorption values of the Ir-$ZrO_2$ catalyst are higher than those of the Ir-$TiO_2$ catalyst. Increasing the reduction temperature results in lower values, which are also likely due to the reduction of the supports close to the active metal because of the strong support to metal interactions, as observed for the Pt systems [43]. The Ir metal becomes decorated by partially reduced oxides that migrate towards/onto the metal, suppressing the chemisorption capacity seen in Table 3 at higher reduction temperatures. The results obtained can be related to those from the TPR experiments, where the support shows the reduction that Ir catalyses at higher reduction temperature. These supports on their own showed no reduction and, according to reported data, these reductions would occur at temperatures beyond 500 °C [33,35].

**Table 3.** CO chemisorption data of the Ir-$TiO_2$ and Ir-$ZrO_2$ catalysts.

| Catalysts | Properties | Temperature of Reduction | | |
|---|---|---|---|---|
| | | **200 °C** | **370 °C** | **500 °C** |
| Ir-$TiO_2$ | Metal dispersion (%) | 61.4 | 52.1 | 36.3 |
| | Metallic surface area ($m^2$/g metal) | 107.9 | 89.4 | 73.3 |
| | Crystallite size (nm) | 6.4 | 7.0 | 7.0 |
| | Chemisorption capacity (CO/Ir) | 0.49 | 0.31 | 0.24 |
| Ir-$ZrO_2$ | Metal dispersion (%) | 91.4 | 77.5 | 54.0 |
| | Metallic surface area ($m^2$/g metal) | 160.6 | 133.0 | 109.1 |
| | Crystallite size (nm) | 5.3 | 5.8 | 5.9 |
| | Chemisorption capacity (CO/Ir) | 0.69 | 0.44 | 0.35 |

#### 2.1.7. Electron Microscopy

Transmission Electron Microscopic images of the supported Ir catalysts are shown in Figure 7, with inserts showing the selected area diffraction patterns, indicating that the samples have a crystalline nature. Particle sizes presented for the oxide phases were similar on both supports at ±7 nm. Figure S4 (ESM) shows the particle size distribution over these catalysts. It could be observed that both the catalysts had a high number of particles with a particle size ranging from 5 nm to 9 nm. These were clearly distinguished from the supports by the lattice fringes in the images presented. These particles are also within a reported particle size range (6–7 nm) for supported Ir catalysts calcined at 400 °C [38].

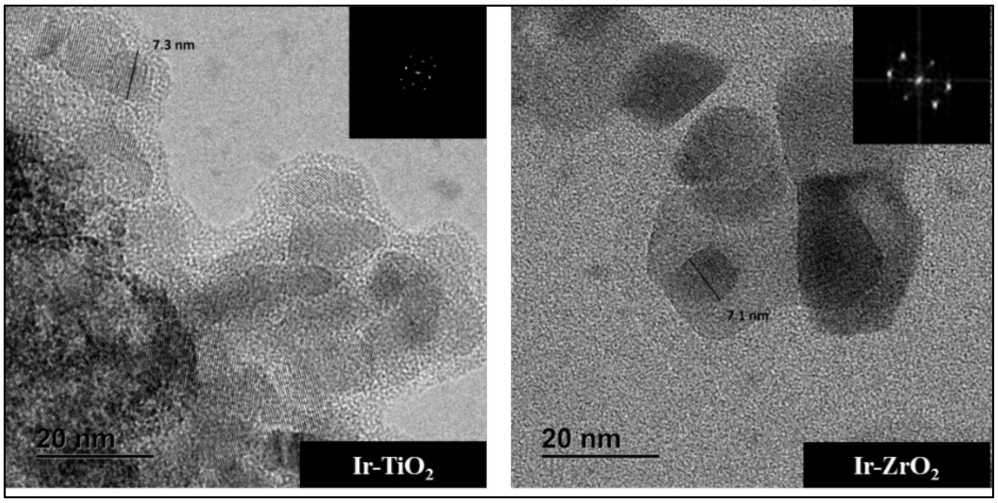


**Figure 7.** HRTEM images of the Ir catalysts (Inset: selected area diffractions).

### *2.2. Catalytic Testing*

#### 2.2.1. CO Oxidation

The activity for the catalysts towards the oxidation of CO in an $H_2$ free feed is shown in Figure 8. The onset temperature for the oxidation reaction starts at 80 °C. After 120 °C, the Ir-$TiO_2$ catalyst shows slightly higher conversions than the Ir-$ZrO_2$ catalyst. Both catalysts reach maximum CO conversions at 200 °C, using stoichiometric amounts of $O_2$ in the feed (ESM, Figure S5). A high CO conversion of ~80% was obtained over Ir-$TiO_2$, while Ir-$ZrO_2$ showed a slightly lower conversion of ~70%. The bare supports, i.e., $TiO_2$ and $ZrO_2$, showed no CO, $O_2$, and $H_2$ conversions during this study.

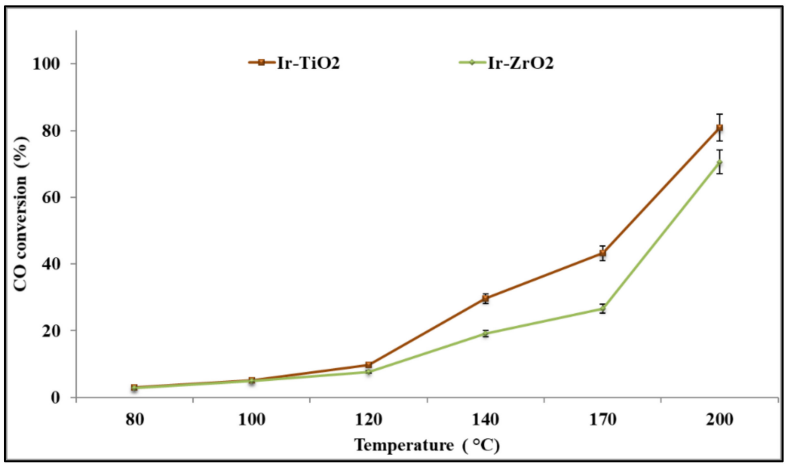


**Figure 8.** CO oxidation reactions over the catalysts with increasing temperatures (GHSV 12,000 $h^{-1}$).

### 2.2.2. PROX Reaction

The catalyst activity of the Ir supported on $TiO_2$ and $ZrO_2$ catalysts for the PROX reaction with a high $H_2$ concentration (50%), is presented in Figure 9. The accompanying $O_2$ conversions are shown in the electronic Supplementary Materials, Figure S4. Both the catalysts are active at temperatures lower than 80 °C (Figure 9). A highest CO conversion of 6.4%, with a selectivity towards $CO_2$ of ~20%, was obtained at a temperature of 80 °C. At temperatures greater than 80 °C, the conversion of CO decreases to ~1% and remains constant, while $CO_2$ selectivity decreases significantly. The Ir-$ZrO_2$ catalyst, on the other hand, shows an increase in CO conversion with increasing temperature from 80 °C, and reaches a maximum of ~20% at 200 °C. The $CO_2$ selectivity for this catalyst was at its highest at 80 °C, and thereafter also decreased with increasing temperature, indicating that the oxidation of $H_2$ becomes more favourable. This is also evident from the $O_2$ conversions shown for the catalysts (ESM, Figure S4).

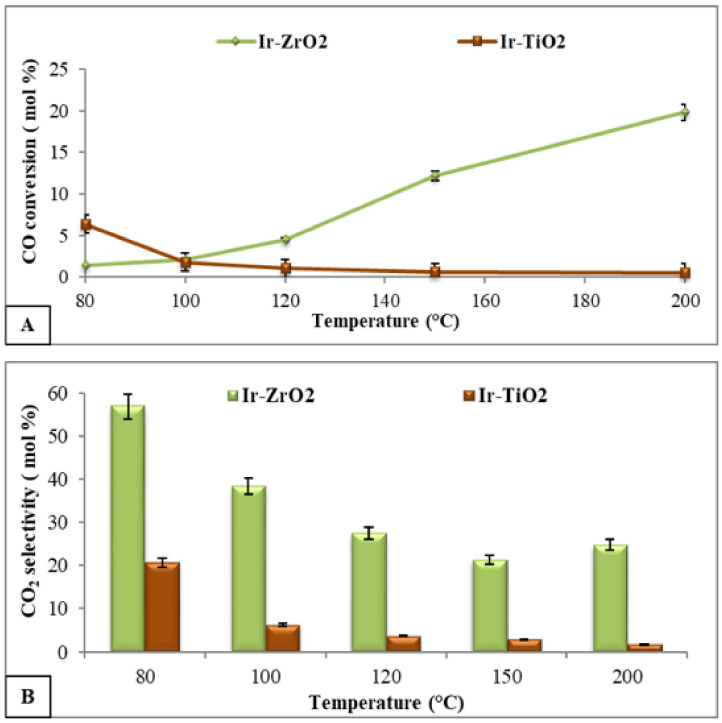


**Figure 9.** CO conversions (**A**) and selectivity towards $CO_2$ (**B**) for the $TiO_2$ and $ZrO_2$ supported Ir catalysts (GHSV 12,000 $h^{-1}$).

The PROX reaction results, obtained over the supported Ir catalysts, relate to those obtained for supported Pt-$TiO_2$ catalysts. The trends based on the supports are almost identical, indicating that the behaviour of these supported catalysts is controlled by the redox properties of the active metals present on them. These results match those obtained from TPR, TPO and CO chemisorption, where the Ir-$TiO_2$ catalyst with a lower reducibility profile, higher oxidation profile, and lower chemisorption values than the Ir-$ZrO_2$ catalyst, was inferior for the PROX reaction. These findings relate closely to reports where $ZrO_2$, being a "hardier" (less easily reduced) support compared to $TiO_2$, is shown to have a stronger interaction between the support and the active metal [33,41–44]. Recently, Coletta et al. [45] stated that high activity in CO conversion could be related to the high metallic dispersion over the catalyst support. Thus, the higher activity of the catalyst could be related to the high Ir site dispersion on the support surface.

The low activity found for these catalysts could likely be occurring by a redox mechanism between CO and O2, similar to that of $H_2$ and $O_2$, over the Ir-$TiO_2$ catalyst, following the Mars and van Krevelen (MvK) mechanism. The $O_2$ conversion confirms this result for the catalyst (ESM, Figure S4), where high conversions > 90% are observed but with very low CO conversions. In general, the CO conversions depend on the oxygen storage capacity, or the available oxygen vacancies, of the catalyst. The $O_2$-TPO profiles show that both the catalysts reoxidise even at room temperature, which could be due to the high number of oxygen vacancies. In general, the stoichiometric conversion ratio between CO and $O_2$ is 1:0.5, which shows that each mole of CO needs an oxygen vacancy for the complete conversion. Thus, the present catalyst with a high number of oxygen vacancies showed a high conversion of CO. The high oxygen conversions also support this.

The Ir-$ZrO_2$ catalyst, on the other hand, allows adsorbed CO to interact with molecular $O_2$ from the feed following the Langmuir–Hinshelwood (LH) mechanism, similar to that of the Pt-$ZrO_2$ catalysts shown in our previous study [11]. A study by Huang et al. [17] reported a non-competitive LH mechanism for a 1.6 wt.% Ir-$CeO_2$ catalyst, where Ir particles themselves were involved in both the CO and $H_2$ oxidation pathways. However, Ir becomes too active to selectively oxidise CO with increasing temperatures and favours $H_2$ oxidation instead, which is evident in this study where $CO_2$ selectivity decreases with increasing temperature (Figure 9). The $H_2$ conversions confirm this over the catalysts (ESM, Figure S5), which show an increase in temperature. Ir-$TiO_2$ shows a higher $H_2$ conversion than the Ir-$ZrO_2$ catalyst, though the CO conversions were much lower.

Another study by Okumura et al. [46] reported that a 1.8 wt.% Ir-$TiO_2$ catalyst synthesised at pH 7, where the point of zero charges of $TiO_2$ was controlled (negatively charged) for better interaction with an $Ir^{4+}$ salt, giving higher stabilities for the catalysts at 27 °C using a feed consisting of 1% CO balanced with air. However, this catalyst still deactivated rapidly after 7h. Comparing these findings with this study, firstly, the amount of $O_2$ used is too high for fuel cell application, where this catalyst would give much higher $H_2$ oxidation. Secondly, the catalyst was not stable for the reaction and showed rapid deactivation early in the reaction. Lastly, the temperature at which maximum CO conversions were obtained was 27 °C, and an onboard fuel cell operates at 80 °C; therefore, by adding to the $O_2$ that is supplied, a heat exchanger would need to be introduced.

For the reactions carried out in this study, the catalysts were stable over the entire heating cycle, irrespective of the low CO conversions. Upon cooling, the results obtained were very similar, showing no signs of deactivation. However, the Ir-$ZrO_2$ catalyst was much more effective than the Ir-$TiO_2$ catalyst. Future work on these materials, such as varying the particle size, support, and pre-treatments, could show promising results towards the oxidation reaction in the presence of $H_2$.

#### 2.2.3. Hydrogenation Reactions

Figure 10 shows the CO hydrogenation reaction profiles over the Ir supported on $TiO_2$ and $ZrO_2$ catalysts. It is seen that these catalysts are active for the hydrogenation reaction, with the onset of activity after 200 °C over both the catalysts. Temperatures above

200 °C for these reactions, unlike the PROX reaction, pose no complications, such as the unwanted oxidation of $H_2$, since no $O_2$ is present in the feed. With an increase in the reaction temperature, the CO conversions of both the catalysts increase accordingly. The Ir-$ZrO_2$ catalyst reached maximum CO conversions of 99.9% at 350 °C, and this remained constant to 370 °C. The Ir-$TiO_2$ catalyst, in contrast, reached a maximum CO conversion at 370 °C of ~88%. The selectivity towards $CH_4$ for both these catalysts were above 90% for all the reaction temperatures investigated, indicating that these catalysts enhance CO methanation compared to WGS. Hydrogen conversions, shown in Figure 10, indicate that only a small fraction of the $H_2$ is used at these high CO conversions. Also, any $CH_4$ formed by CO conversion can be reused in the reformer for onboard applications, therefore, $H_2$ loss remains minimal [47].

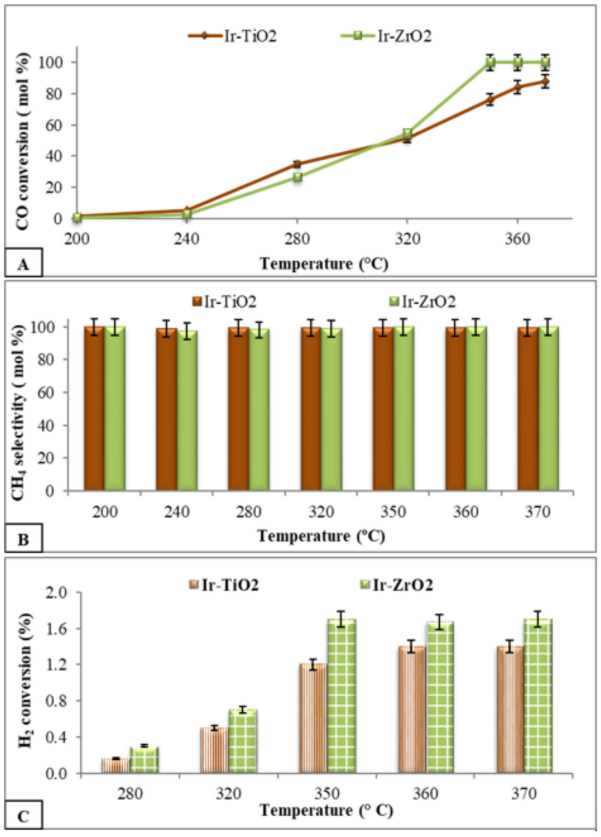


**Figure 10.** CO hydrogenation reaction over the $TiO_2$ and $ZrO_2$ supported catalysts with increasing temperatures, CO conversion (**A**), $CH_4$ selectivity (**B**) and $H_2$ conversion (**C**) (GHSV 12,000 $h^{-1}$).

The Ir-$ZrO_2$ catalyst showed better CO chemisorption capacity, metallic surface area, metal dispersion, smaller particle sizes, and thus better catalytic activity, than the Ir-$TiO_2$ catalyst, due to the strong metal support interactions of $ZrO_2$ and Ir, which resulted from controlling the IEP during the synthesis, which gave better metal support interactions. The availability of active metal for CO hydrogenation on the Ir-$ZrO_2$ catalyst at higher temperatures was enhanced compared to the Ir-$TiO_2$ catalyst. Furthermore, there is evidence of CO adsorption (CO chemisorption) still taking place on both the catalysts at higher temperatures, even past the hydrogenation reaction at 500 °C, which reveals that Ir active sites are still available and not completely embedded in the support. Following the high-temperature WGS reaction, these Ir catalysts may have the promise to remove the trace CO present in the reformate gas.

## 3. Materials and Methods

Commercial Titania (99.7% metal basis, Alfa Aesar) and Zirconia (99.7% metal basis, Alfa Aesar) were used in this study. All catalysts were prepared by the deposition–precipitation technique [48]. The prepared catalysts were characterised by using physisorption, chemisorption, diffraction, spectroscopic, and microscopic techniques. The catalytic testing was performed in a continuous flow fixed bed reactor in a downflow mode at atmospheric pressure. The inlet and outlet gaseous products of the reactor were analysed on an online Agilent Micro-GC CP-4900 TCD housing 3 channels. The amount of CO and $H_2$ converted during the reaction was calculated on the basis of inlet and outlet gas concentrations [49]. The detailed procedures for the catalyst synthesis, catalyst characterisation, and catalytic testing are given in the Electronic Supplementary Materials to this paper (ESM, Sections S1–S3).

## 4. Conclusions

All catalysts were active for the oxidation of CO, showing significant activity in the temperature range screened (80–200 °C). However, both the catalysts showed low activity for the PROX reactions since the oxidation of $H_2$ was favoured, as opposed to the desired CO oxidation. Characterisation data of the prepared catalysts showed that supports with well-dispersed Ir particles formed interstitials ($O_2$ vacancies) due to the strong metal–support interactions at the interface. These interactions allow for partial reduction of the supports which the Ir catalyses on the surface. Therefore, $H_2$ reacts with $O_2$, forming $H_2O$ instead of $CO_2$ in the PROX reaction. The Ir-$TiO_2$ catalyst follows the Mars and van Krevelen pathway, using lattice oxygen for the oxidation reaction, while the Ir-$ZrO_2$ catalysts follow the Langmuir–Hinshelwood pathway.

The results are promising for both Ir supported on $TiO_2$ and $ZrO_2$ catalysts with respect to lowering the quantity of CO in reformate gas to low ppm levels by CO hydrogenation. Ir-$ZrO_2$ gave 99.9% CO conversion above 350 °C, with high $CH_4$ selectivity. Controlling the IEP of the catalysts during the synthesis resulted in better dispersion of Ir over the supports, thus favouring the interaction between metal and support. $TiO_2$ and $ZrO_2$ supported Ir catalysts prepared by the deposition–precipitation method show promising activity for the hydrogenation of CO, following the high temperature WGS reaction for removing trace quantities of CO. These catalysts now need to be subjected to ideal exit WGS reformate feeds for further investigation to determine the catalyst's stability in the presence of $CO_2$ and $H_2O$.

**Supplementary Materials:** The following are available online at https://www.mdpi.com/article/10.3390/catal11111378/s1, Figure S1. XRD diffractograms of the supports and catalysts; Figure S2. XPS spectra showing the Zr 3d5/2, Ti 2p3/2 and the O 1s levels for the catalysts; Figure S3. FTIR-CO analyses of the catalysts with increasing temperatures; Figure S4. $O_2$ conversions of the supported Ir catalysts for (A): Total oxidation and (B): PROX; Figure S5. $H_2$ conversions of the supported Ir catalysts for the PROX reaction.

**Author Contributions:** Conceptualization, Z.M., V.D.B.C.D., S.S. and H.B.F.; Methodology, Z.M., V.D.B.C.D., S.S. and H.B.F.; Validation, V.D.B.C.D. and S.S.; Formal Analysis, Z.M. and V.D.B.C.D.; Investigation, Z.M. and V.D.B.C.D.; Resources, H.B.F.; Data Curation, Z.M. and V.D.B.C.D.; Writing—Original Draft Preparation, Z.M. and V.D.B.C.D.; Writing—Review & Editing, S.S. and H.B.F.; Visualization, Z.M., S.S. and H.B.F.; Supervision, S.S. and H.B.F.; Project Administration, S.S. and H.B.F.; Funding Acquisition, H.B.F.; All authors have read and agreed to the published version of the manuscript.

**Funding:** This research was funded by NRF (grant number 118527) and HySA (grant number H977).

**Data Availability Statement:** Data is contained within the article and the Supplementary Materials.

**Acknowledgments:** The NRF and HySA are thanked for financial support. We further thank J. Wesley-Smith (CSIR, RSA) for the microscopic imaging, D. Morgan (Cardiff Catalysis Institute, UK) for support with the XPS studies, P. Mohlala and M. du Toit (SASOL R&T, RSA) for the FTIR-CO data.

**Conflicts of Interest:** The authors declare no conflict of interest.

## References

1. Lin, L.; Yao, S.; Gao, R.; Liang, X.; Yu, Q.; Deng, Y.; Liu, J.; Peng, M.; Jiang, Z.; Li, S.; et al. A highly CO-tolerant atomically dispersed Pt catalyst for chemoselective hydrogenation. *Nat. Nanotechnol.* **2019**, *14*, 354–361. [CrossRef]
2. Mohammedi, A.; Sahli, Y.; Ben Moussa, H. 3D investigation of the channel cross-section configuration effect on the power delivered by PEMFCs with straight channels. *Fuel* **2020**, *263*, 116713. [CrossRef]
3. Moreno, M.; Baronetti, G.T.; Laborde, M.A.; Mariño, F.J. Kinetics of preferential CO oxidation in $H_2$ excess (COPROX) over $CuO/CeO_2$ catalysts. *Int. J. Hydrogen Energy* **2008**, *33*, 3538–3542. [CrossRef]
4. Park, E.D.; Lee, D.; Lee, H.C. Recent progress in selective CO removal in a $H_2$-rich stream. *Catal. Today* **2009**, *139*, 280–290. [CrossRef]
5. Panagiotopoulou, P.; Kondarides, D.I.; Verykios, X.E. Selective methanation of CO over supported Ru catalysts. *Appl. Catal. B* **2009**, *88*, 470–478. [CrossRef]
6. Tada, S.; Kikuchi, R.; Takagaki, A.; Sugawara, T.; Ted Oyama, S.; Satokawa, S. Effect of metal addition to $Ru/TiO_2$ catalyst on selective CO methanation. *Catal. Today* **2014**, *232*, 16–21. [CrossRef]
7. Ahluwalia, R.K.; Zhang, Q.; Chmielewski, D.J.; Lauzze, K.C.; Inbody, M.A. Performance of CO preferential oxidation reactor with noble-metal catalyst coated on ceramic monolith for onboard fuel processing applications. *Catal. Today* **2005**, *99*, 271–283. [CrossRef]
8. Dasireddy, V.D.B.C.; Hajduk, Š.; Ruiz-Zepeda, F.; Kovač, J.; Likozar, B.; Orel, Z.C. $CeO_2$ and $TiO_2$ support material effects on NH3 decomposition pathway mechanism over Cu–Zn catalysts. *Fuel Process. Technol.* **2021**, *215*, 106752. [CrossRef]
9. Di, L.; Wu, G.; Dai, W.; Guan, N.; Li, L. $Ru/TiO_2$ for the preferential oxidation of CO in $H_2$-rich stream: Effects of catalyst pre-treatments and reconstruction of Ru sites. *Fuel* **2015**, *143*, 318–326. [CrossRef]
10. Eckle, S.; Anfang, H.-G.; Behm, R.J. What drives the selectivity for CO methanation in the methanation of $CO_2$-rich reformate gases on supported Ru catalysts? *Appl. Catal. A* **2011**, *391*, 325–333. [CrossRef]
11. Mohamed, Z.; Dasireddy, V.D.B.C.; Singh, S.; Friedrich, H.B. The preferential oxidation of CO in hydrogen rich streams over platinum doped nickel oxide catalysts. *Appl. Catal. B Environ.* **2016**, *180*, 687–697. [CrossRef]
12. Kim, Y.H.; Park, J.E.; Lee, H.C.; Choi, S.H.; Park, E.D. Active size-controlled Ru catalysts for selective CO oxidation in $H_2$. *Appl. Catal. B Environ.* **2012**, *127*, 129–136. [CrossRef]
13. Mariño, F.; Descorme, C.; Duprez, D. Noble metal catalysts for the preferential oxidation of carbon monoxide in the presence of hydrogen (PROX). *Appl. Catal. B Environ.* **2004**, *54*, 59–66. [CrossRef]
14. Tada, S.; Minori, D.; Otsuka, F.; Kikuchi, R.; Osada, K.; Akiyama, K.; Satokawa, S. Effect of Ru and Ni ratio on selective CO methanation over $Ru\text{-}Ni/TiO_2$. *Fuel* **2014**, *129*, 219–224. [CrossRef]
15. Mohamed, Z.; Dasireddy, V.D.B.C.; Singh, S.; Friedrich, H.B. $TiO_2$ and $ZrO_2$ supported Ru catalysts for CO mitigation following the water-gas shift reaction. *Int. J. Hydrogen Energy* **2018**, *43*, 22291–22302. [CrossRef]
16. Dasireddy, V.D.B.C.; Likozar, B. Direct methanol production from mixed methane/$H_2O$/$N_2O$ feedstocks over $Cu–Fe/Al_2O_3$ catalysts. *Fuel* **2021**, *301*, 121084. [CrossRef]
17. Huang, Y.; Wang, A.; Wang, X.; Zhang, T. Preferential oxidation of CO under excess $H_2$ conditions over iridium catalysts. *Int. J. Hydrogen Energy* **2007**, *32*, 3880–3886. [CrossRef]
18. Nguyen, T.-S.; Morfin, F.; Aouine, M.; Bosselet, F.; Rousset, J.-L.; Piccolo, L. Trends in CO oxidation and PROX performances of the platinum-group metals supported on ceria. *Catal. Today* **2015**, *253*, 106–114. [CrossRef]
19. Doustkhah, E.; Assadi, M.H.N.; Komaguchi, K.; Tsunoji, N.; Esmat, M.; Fukata, N.; Tomita, O.; Abe, R.; Ohtani, B.; Ide, Y. In situ Blue titania via band shape engineering for exceptional solar $H_2$ production in rutile $TiO_2$. *Appl. Catal. B Environ.* **2021**, *297*, 120380. [CrossRef]
20. Sing, K.S.W.; Everett, D.H.; Haul, R.A.W.; Moscou, L.; Pierotti, R.A.; Rouquerol, J.; Siemieniewska, T. Reporting physisorption data for gas/solid systems with special reference to the determination of surface area and porosity (Recommendations 1984). *Pure Appl. Chem.* **1985**, *57*, 603–619. [CrossRef]
21. Campos, C.; Torres, C.; Oportus, M.; Pena, M.A.; Fierro, J.L.G.; Reyes, P. Hydrogenation of substituted aromatic nitrobenzenes over 1% 1.0 wt.% $Ir/ZrO_2$ catalyst: Effect of meta position and catalytic performance. *Catal. Today* **2013**, *213*, 93–100. [CrossRef]
22. Dasireddy, V.D.B.C.; Neja, S.Š.; Blaž, L. Correlation between synthesis pH, structure and $Cu/MgO/Al_2O_3$ heterogeneous catalyst activity and selectivity in $CO_2$ hydrogenation to methanol. *J. $CO_2$ Util.* **2018**, *28*, 189–199. [CrossRef]
23. Dasireddy, V.D.B.C.; Štefančič, N.S.; Huš, M.; Likozar, B. Effect of alkaline earth metal oxide (MO) $Cu/MO/Al_2O_3$ catalysts on methanol synthesis activity and selectivity via $CO_2$ reduction. *Fuel* **2018**, *233*, 103–112. [CrossRef]
24. Yoshida, A.; Mori, Y.; Ikeda, T.; Azemoto, K.; Naito, S. Enhancement of catalytic activity of $Ir/TiO_2$ by partially reduced titanium oxide in aerobic oxidation of alcohols. *Catal. Today* **2013**, *203*, 153–157. [CrossRef]

25. Feng, W.; Wu, G.; Li, L.; Guan, N. Solvent-free selective photocatalytic oxidation of benzyl alcohol over modified $TiO_2$. *Green Chem.* **2011**, *13*, 3265–3272. [CrossRef]
26. Rojas, H.; Borda, G.; Reyes, P.; Martinez, J.J.; Valencia, J.; Fierro, J.L.G. Citral hydrogenation over $Ir/TiO_2$ and $Ir/TiO_2/SiO_2$ catalysts. *Catal. Today* **2008**, *133–135*, 699–705. [CrossRef]
27. Vicerich, M.A.; Oportus, M.; Benitez, V.M.; Reyes, P.; Pieck, C.L. Influence of Na content on the catalytic properties of $Pt\text{-}Ir/Al_2O_3$ catalysts for selective ring opening of decalin. *Appl. Catal. A* **2014**, *480*, 42–49. [CrossRef]
28. Azzam, K.G.; Babich, I.V.; Seshan, K.; Lefferts, L. A bifunctional catalyst for the single-stage water–gas shift reaction in fuel cell applications. Part 2. Roles of the support and promoter on catalyst activity and stability. *J. Catal.* **2007**, *251*, 163–171. [CrossRef]
29. Zhang, C.; He, H.; Tanaka, K.-i. Catalytic performance and mechanism of a $Pt/TiO_2$ catalyst for the oxidation of formaldehyde at room temperature. *Appl. Catal. B Environ.* **2006**, *65*, 37–43. [CrossRef]
30. Panagiotopoulou, P.; Christodoulakis, A.; Kondarides, D.I.; Boghosian, S. Particle size effects on the reducibility of titanium dioxide and its relation to the water–gas shift activity of $Pt/TiO_2$ catalysts. *J. Catal.* **2006**, *240*, 114–125. [CrossRef]
31. Dasireddy, V.D.B.C.; Likozar, B. Activation and Decomposition of Methane over Cobalt-, Copper-, and Iron-Based Heterogeneous Catalysts for COx-Free Hydrogen and Multiwalled Carbon Nanotube Production. *Energy Technol.* **2017**, *5*, 1344–1355. [CrossRef]
32. Hajduk, Š.; Dasireddy, V.D.B.C.; Likozar, B.; Dražić, G.; Orel, Z.C. COx-free hydrogen production via decomposition of ammonia over Cu–Zn-based heterogeneous catalysts and their activity/stability. *Appl. Catal. B Environ.* **2017**, *211*, 57–67. [CrossRef]
33. Benvenutti, E.V.; Franken, L.; Moro, C.C.; Davanzo, C.U. FTIR Study of Hydrogen and Carbon Monoxide Adsorption on $Pt/TiO_2$, $Pt/ZrO_2$, and $Pt/Al_2O_3$. *Langmuir* **1999**, *15*, 8140–8146. [CrossRef]
34. Pesty, F.; Steinrueck, H.-P.; Madey, T.E. Thermal stability of Pt films on $TiO_2$(110): Evidence for encapsulation. *Surf. Sci.* **1995**, *339*, 83–95. [CrossRef]
35. Hwang, K.-R.; Ihm, S.-K.; Park, S.-C.; Park, J.-S. $Pt/ZrO_2$ catalyst for a single-stage water-gas shift reaction: Ti addition effect. *Int. J. Hydrogen Energy* **2013**, *38*, 6044–6051. [CrossRef]
36. Mohamed, Z.; Dasireddy, V.D.B.C.; Singh, S.; Friedrich, H.B. Comparative studies for CO oxidation and hydrogenation over supported Pt catalysts prepared by different synthesis methods. *Renew. Energy* **2020**, *148*, 1041–1053. [CrossRef]
37. Gao, Y.; Xie, K.; Mi, S.; Liu, N.; Wang, W.; Huang, W. Preferential oxidation of CO in a $H_2$-rich stream over multi-walled carbon nanotubes confined Ru catalysts. *Int. J. Hydrogen Energy* **2013**, *38*, 16665–16676. [CrossRef]
38. Amrousse, R.; Hori, K.; Fetimi, W. Iridium dispersion control in $Ir/Al_2O_3\text{-}SiO_2$ catalysts by calcination temperature using chloroiridic acid as catalyst precursor. *Catal. Commun.* **2012**, *27*, 174–178. [CrossRef]
39. Bourane, A.; Nawdali, M.; Bianchi, D. Heats of Adsorption of the Linear CO Species Adsorbed on a $Ir/Al_2O_3$ Catalyst Using in Situ FTIR Spectroscopy under Adsorption Equilibrium. *J. Phys. Chem. B* **2002**, *106*, 2665–2671. [CrossRef]
40. Chen, P.; Lu, J.-Q.; Xie, G.-Q.; Hu, G.-S.; Zhu, L.; Luo, L.-F.; Huang, W.-X.; Luo, M.-F. Effect of reduction temperature on selective hydrogenation of crotonaldehyde over $Ir/TiO_2$ catalysts. *Appl. Catal. A* **2012**, *433–434*, 236–242. [CrossRef]
41. Ruppert, A.M.; Paryjczak, T. $Pt/ZrO_2/TiO_2$ catalysts for selective hydrogenation of crotonaldehyde: Tuning the SMSI effect for optimum performance. *App. Catal. A Gen.* **2007**, *320*, 80–90. [CrossRef]
42. Siddiquey, I.A.; Furusawa, T.; Sato, M.; Bahadur, N.M.; Uddin, M.N.; Suzuki, N. A rapid method for the preparation of silica-coated $ZrO_2$ nanoparticles by microwave irradiation. *Ceram. Int.* **2011**, *37*, 1755–1760. [CrossRef]
43. Bitter, J.H.; Seshan, K.; Lercher, J.A. The state of zirconia supported platinum catalysts for $CO_2/CH_4$ reforming. *J. Catal.* **1997**, *171*, 279–286. [CrossRef]
44. Doemoek, M.; Oszko, A.; Baan, K.; Sarusi, I.; Erdohelyi, A. Reforming of ethanol on $Pt/Al_2O_3\text{-}ZrO_2$ catalyst. *Appl. Catal. A* **2010**, *383*, 33–42. [CrossRef]
45. Coletta, V.C.; Gonçalves, R.V.; Bernardi, M.I.B.; Hanaor, D.A.H.; Assadi, M.H.N.; Marcos, F.C.F.; Nogueira, F.G.E.; Assaf, E.M.; Mastelaro, V.R. Cu-Modified $SrTiO_3$ Perovskites Toward Enhanced Water–Gas Shift Catalysis: A Combined Experimental and Computational Study. *ACS Appl. Energy Mater.* **2021**, *4*, 452–461. [CrossRef]
46. Okumura, M.; Masuyama, N.; Konishi, E.; Ichikawa, S.; Akita, T. CO Oxidation below Room Temperature over $Ir/TiO_2$ Catalyst Prepared by Deposition Precipitation Method. *J. Catal* **2002**, *208*, 485–489. [CrossRef]
47. Dagle, R.A.; Wang, Y.; Xia, G.-G.; Strohm, J.J.; Holladay, J.; Palo, D.R. Selective CO methanation catalysts for fuel processing applications. *Appl. Catal. A* **2007**, *326*, 213–218. [CrossRef]
48. Sangeetha, P.; Zhao, B.; Chen, Y.-W. $Au/CuOx{-}TiO_2$ Catalysts for Preferential Oxidation of CO in Hydrogen Stream. *Ind. Eng. Chem. Res.* **2010**, *49*, 2096–2102. [CrossRef]
49. Dasireddy, V.D.B.C.; Likozar, B.; Valand, J. Preferential oxidation of CO in $H_2/H_2O/CO_2$ water–gas shift feedstocks over Cu-based carbon nanotubes-supported heterogeneous catalysts. *Appl. Catal. B Environ.* **2018**, *237*, 1044–1058. [CrossRef]